Biomedical Optics EXPRESS

The use of forward scatter to improve retinal vascular imaging with an adaptive optics scanning laser ophthalmoscope

Toco Y. P. Chui,[1] Dean A. VanNasdale,[1] and Stephen A. Burns[1,*]

[1]*School of Optometry, Indiana University, 800 E Atwater Avenue, Bloomington, IN 47405, USA*
staburns@indiana.edu

Abstract: Retinal vascular diseases are a leading cause of blindness and visual disability. The advent of adaptive optics retinal imaging has enabled us to image the retinal vascular at cellular resolutions, but imaging of the vasculature can be difficult due to the complex nature of the images, including features of many other retinal structures, such as the nerve fiber layer, glial and other cells. In this paper we show that varying the size and centration of the confocal aperture of an adaptive optics scanning laser ophthalmoscope (AOSLO) can increase sensitivity to multiply scattered light, especially light forward scattered from the vasculature and erythrocytes. The resulting technique was tested by imaging regions with different retinal tissue reflectivities as well as within the optic nerve head.

OCIS codes: (110.1085) Adaptive imaging; (110.1220) Apertures; (170.4460) Ophthalmic optics and devices; (170.1470) Blood or tissue constituent monitoring.

References and links

1. J. H. Kempen, B. J. O'Colmain, M. C. Leske, S. M. Haffner, R. Klein, S. E. Moss, H. R. Taylor, and R. F. Hamman; Eye Diseases Prevalence Research Group, "The prevalence of diabetic retinopathy among adults in the United States," Arch. Ophthalmol. **122**(4), 552–563 (2004).
2. N. R. Burrows, I. A. Hora, Y. Li, and J. B. Saaddine; Centers for Disease Control and Prevention (CDC), "Self-reported visual impairment among persons with diagnosed diabetes --- United States, 1997--2010," MMWR Morb. Mortal. Wkly. Rep. **60**(45), 1549–1553 (2011).
3. F. Musa, W. J. Muen, R. Hancock, and D. Clark, "Adverse effects of fluorescein angiography in hypertensive and elderly patients," Acta Ophthalmol. Scand. **84**(6), 740–742 (2006).
4. A. S. Kwan, C. Barry, I. L. McAllister, and I. Constable, "Fluorescein angiography and adverse drug reactions revisited: the Lions Eye experience," Clin. Experiment. Ophthalmol. **34**(1), 33–38 (2006).
5. T. Y. Chui, Z. Zhong, H. Song, and S. A. Burns, "Foveal avascular zone and its relationship to foveal pit shape," Optom. Vis. Sci. **89**(5), 602–610 (2012).
6. J. Tam, J. A. Martin, and A. Roorda, "Noninvasive visualization and analysis of parafoveal capillaries in humans," Invest. Ophthalmol. Vis. Sci. **51**(3), 1691–1698 (2010).
7. R. Ferguson, D. Hammer, A. Elsner, R. Webb, S. Burns, and J. Weiter, "Wide-field retinal hemodynamic imaging with the tracking scanning laser ophthalmoscope," Opt. Express **12**(21), 5198–5208 (2004).
8. D. Y. Kim, J. Fingler, J. S. Werner, D. M. Schwartz, S. E. Fraser, and R. J. Zawadzki, "*In vivo* volumetric imaging of human retinal circulation with phase-variance optical coherence tomography," Biomed. Opt. Express **2**(6), 1504–1513 (2011).
9. S. Zotter, M. Pircher, T. Torzicky, M. Bonesi, E. Götzinger, R. A. Leitgeb, and C. K. Hitzenberger, "Visualization of microvasculature by dual-beam phase-resolved Doppler optical coherence tomography," Opt. Express **19**(2), 1217–1227 (2011).
10. S. Makita, F. Jaillon, M. Yamanari, and Y. Yasuno, "Dual-beam-scan Doppler optical coherence angiography for birefringence-artifact-free vasculature imaging," Opt. Express **20**(3), 2681–2692 (2012).
11. A. Szkulmowska, M. Szkulmowski, D. Szlag, A. Kowalczyk, and M. Wojtkowski, "Three-dimensional quantitative imaging of retinal and choroidal blood flow velocity using joint Spectral and Time domain Optical Coherence Tomography," Opt. Express **17**(13), 10584–10598 (2009).
12. L. An and R. K. Wang, "*In vivo* volumetric imaging of vascular perfusion within human retina and choroids with optical micro-angiography," Opt. Express **16**(15), 11438–11452 (2008).
13. M. Hogan, J. Alvarado, and J. Weddell, in *Histology of the Human Eye* (W.B. Saunders, Philadelphia, 1971), pp. 523–606.

#173363 - $15.00 USD Received 2 Aug 2012; rev. 10 Sep 2012; accepted 10 Sep 2012; published 13 Sep 2012

14. D. Scoles, D. C. Gray, J. J. Hunter, R. Wolfe, B. P. Gee, Y. Geng, B. D. Masella, R. T. Libby, S. Russell, D. R. Williams, and W. H. Merigan, "*In-vivo* imaging of retinal nerve fiber layer vasculature: imaging histology comparison," BMC Ophthalmol. **9**(1), 9 (2009).
15. A. E. Elsner, S. A. Burns, J. J. Weiter, and F. C. Delori, "Infrared imaging of sub-retinal structures in the human ocular fundus," Vision Res. **36**(1), 191–205 (1996).
16. A. Elsner, M. Miura, S. Burns, E. Beausencourt, C. Kunze, L. Kelley, J. Walker, G. Wing, P. Raskauskas, D. Fletcher, Q. Zhou, and A. Dreher, "Multiply scattered light tomography and confocal imaging: detecting neovascularization in age-related macular degeneration," Opt. Express **7**(2), 95–106 (2000).
17. R. D. Ferguson, Z. Zhong, D. X. Hammer, M. Mujat, A. H. Patel, C. Deng, W. Zou, and S. A. Burns, "Adaptive optics scanning laser ophthalmoscope with integrated wide-field retinal imaging and tracking," J. Opt. Soc. Am. A **27**(11), A265–A277 (2010).
18. A. E. Elsner, A. Weber, M. C. Cheney, D. A. VanNasdale, and M. Miura, "Imaging polarimetry in patients with neovascular age-related macular degeneration," J. Opt. Soc. Am. A **24**(5), 1468–1480 (2007).
19. American National Standard Institute, American National Standard for the Safe Use of Lasers, ANSI Z136.1–2007 (ANSI, New York, 2007).
20. Y. N. Sulai and A. Dubra, "Adaptive optics scanning ophthalmoscopy with annular pupils," Biomed. Opt. Express **3**(7), 1647–1661 (2012).
21. S. A. Burns, A. E. Elsner, M. B. Mellem-Kairala, and R. B. Simmons, "Improved contrast of subretinal structures using polarization analysis," Invest. Ophthalmol. Vis. Sci. **44**(9), 4061–4068 (2003).
22. A. Weber, M. Cheney, Q. Smithwick, and A. Elsner, "Polarimetric imaging and blood vessel quantification," Opt. Express **12**(21), 5178–5190 (2004).
23. S. A. Burns, R. Tumbar, A. E. Elsner, D. Ferguson, and D. X. Hammer, "Large-field-of-view, modular, stabilized, adaptive-optics-based scanning laser ophthalmoscope," J. Opt. Soc. Am. A **24**(5), 1313–1326 (2007).
24. J. Q. Lu, P. Yang, and X. H. Hu, "Simulations of light scattering from a biconcave red blood cell using the finite-difference time-domain method," J. Biomed. Opt. **10**(2), 024022 (2005).
25. J. Liang, D. R. Williams, and D. T. Miller, "Supernormal vision and high-resolution retinal imaging through adaptive optics," J. Opt. Soc. Am. A **14**(11), 2884–2892 (1997).
26. S. S. Choi, N. Doble, J. L. Hardy, S. M. Jones, J. L. Keltner, S. S. Olivier, and J. S. Werner, "*In vivo* imaging of the photoreceptor mosaic in retinal dystrophies and correlations with visual function," Invest. Ophthalmol. Vis. Sci. **47**(5), 2080–2092 (2006).
27. P. Henkind, "Radial peripapillary capillaries of the retina. I. Anatomy: human and comparative," Br. J. Ophthalmol. **51**(2), 115–123 (1967).
28. M. J. Hogan and L. Feeney, "The ultrastructure of the retinal blood vessels. I. The large vessels," J. Ultrastruct. Res. **9**(1-2), 10–28 (1963).
29. Z. Zhong, B. L. Petrig, X. Qi, and S. A. Burns, "*In vivo* measurement of erythrocyte velocity and retinal blood flow using adaptive optics scanning laser ophthalmoscopy," Opt. Express **16**(17), 12746–12756 (2008).
30. A. T. Phan, A. Elsner, T. Y. Chui, D. VanNasdale, C. A. Clark, V. E. Malinovsky, and S. A. Burns, "*In vivo* microvascular changes in diabetic patients without clinically severe diabetic retinopathy," presented at the 2012 ARVO Annual Meeting—Association for Research in Vision and Ophthalmology, Fort Lauderdale, FL, 5–10 May 2012.
31. O. Y. Tektas, E. Lütjen-Drecoll, and M. Scholz, "Qualitative and quantitative morphologic changes in the vasculature and extracellular matrix of the prelaminar optic nerve head in eyes with POAG," Invest. Ophthalmol. Vis. Sci. **51**(10), 5083–5091 (2010).
32. A. L. Kornzweig, I. Eliasoph, and M. Feldstein, "Selective atrophy of the radial peripapillary capillaries in chronic glaucoma," Arch. Ophthalmol. **80**(6), 696–702 (1968).
33. H. S. Chung, A. Harris, L. Kagemann, and B. Martin, "Peripapillary retinal blood flow in normal tension glaucoma," Br. J. Ophthalmol. **83**(4), 466–469 (1999).

1. Introduction

The ability to image the complex retinal microvasculature network is an important step in advancing our understanding of normal structure and function as well as pathological changes associated with sight-threatening retinal disease. Retinal vascular diseases such as diabetes are the major causes of blindness in the developed world [1,2]. Although compromised retinal vascular structure and retinal blood flow have been reported in retinal diseases, our ability to image the retinal vasculature *in vivo* typically requires the injection of exogenous dyes such as sodium fluorescein or indocyanine green to enhance the normally low contrast found in the retinal tissues. This is expensive, time intensive, and carries significant systemic risks in a small proportion of the population [3,4]. Recently, advances in both direct detection techniques [5–7] and coherent detection techniques [8–12] have expanded our ability to map the retinal vasculature, but these techniques use variations over time to perform the mapping and do not provide an enhanced visualization of the vascular structures themselves.

#173363 - $15.00 USD Received 2 Aug 2012; rev. 10 Sep 2012; accepted 10 Sep 2012; published 13 Sep 2012

The larger arteries and veins in human retina are readily visible with low resolution imaging techniques. The smaller arterioles, capillaries, and venules are much more difficult to visualize, which can be partially overcome with the use of high resolution imaging techniques. Recently, the AOSLO has allowed noninvasive visualization and quantification of the foveal and parafoveal capillary network in living human retina without the injection of contrast agents, using blood flow as a surrogate marker for vascular structure [5,6]. Noninvasive imaging of the peripapillary, papillary, and perifoveal (~5°–10° from the fovea) [13] microvascular networks remains challenging however, because of the complexity of the retina, and confocal images focused on the vasculature include many structures, including the retinal nerve fiber layer (RNFL) and other non-neural components including glial cells. These structures can also return a strong backscattering signal to the detector via a confocal aperture conjugated with the retinal plane and their presence can mask the appearance of the microvasculature. Combining fluorescein angiography and AOSLO, it is now possible to visualize the peripapillary microvascular network in macaque retina [14]. Unfortunately, this imaging technique has not yet been applied in living human retina due to the invasive nature and the relatively long imaging session. In this paper, we present the use of an imaging approach that emphasizes multiple light scattering [15,16] instead of direct backscatter to improve visualization of the peripapillary, papillary, and perifoveal microvascular network in living human retina. This is done without the use of contrast agents, allowing microvascular examination in both normal and diseased retinas, as frequently as required for clinical or scientific purposes. By systematically varying the position and/or size of our confocal aperture, we determined the conditions producing improved imaging of both erythrocytes and the microvasculature, including the fine structure of arteriole walls.

2. Methods

2.1. Subjects

Six healthy subjects (ages 22–35 yr; 5 males and 1 female) participated in this study. All subjects received a complete eye examination, including a subjective refraction and fundus examination. All subjects had best corrected visual acuity of 20/20 or better. Only one eye of each subject was tested. A 30° × 30° infrared scanning laser ophthalmoscope (SLO) fundus image was obtained for each subject using the Spectralis OCT (Heidelberg Engineering, Heidelberg, Germany). Pupil dilation with 1 drop of 1% tropicamide was performed on all subjects. Informed consent was obtained after a full explanation of the procedures and consequences of the study. This study protocol was approved by the Indiana University Review Board and complied with the requirements of the Declaration of Helsinki.

2.2. AOSLO instrumentation

The Indiana AOSLO used in this experiment has been described in detail previously [17]. In short the AOSLO uses a supercontinuum source (Fianium, Inc.) to provide both the wavefront sensing beacon and the imaging sources. Wavefront sensing was performed at 740 nm, and imaging at 820 nm, with the wavelengths obtained using interference filters with bandwidths of 13 nm and 12 nm, respectively (Semrock, Inc). Light returning from the retina passes through a confocal aperture optically conjugate to the retinal plane. This confocal aperture was approximately 2× or 10× the Airy disk diameter as measured in the detector plane. These values are calculated for the maximal pupil size of our system (8 mm at the eye). In practice not all subjects when dilated reached this pupil size, and in those cases the Airy disk diameter would be slightly larger. Based on the theoretical calculation, the axial resolution was approximately 80 μm for the 2× Airy disk diameter confocal aperture (small aperture) and 150 μm for the 10× Airy disk diameter confocal aperture (large aperture). In this experiment, the vertical scan was programmed to provide full frame images of either 2° × 1.8° or 1.3° ×

#173363 - $15.00 USD Received 2 Aug 2012; rev. 10 Sep 2012; accepted 10 Sep 2012; published 13 Sep 2012

1.2° at a frame rate of 28 Hz. Subject's head movements were stabilized using a chin and head rest.

2.3. Confocal aperture control

Confocal apertures were mounted on a motorized filter wheel which could be rotated to switch between apertures. The motorized filter wheel was mounted on an automated XY positioning stage, allowing translation of the apertures perpendicular to the direction of beam propagation to an accuracy of better than 1 μm. Thus, the apertures were always focused in the same plane as the imaging beam, but their position relative to the focal waist of the imaging beam was varied. Within each imaging session the centered aperture positions were first recalibrated using a model eye to ensure they were confocal with the imaging beam. Center coordinates for the apertures were saved to the control computer. During imaging, changing the aperture size selection caused the control computer to move the translation stage to bring each aperture into confocal alignment in less than 5 seconds. The aperture could then be displaced by the operator while the computer recorded the altered aperture position. The larger confocal aperture was used to capture more multiply scattered light [15]. We also systematically displaced the larger aperture, allowing us to change the relative contributions of multiply scattered [18] and singly scattered light.

Three aperture manipulations were studied. 1. We investigated the effect of aperture size by imaging the same location using the small and large apertures (tested in Subject 1). 2. We varied the large aperture from −8× Airy disk diameter to +8× Airy disk diameter location from its centered position. Displacements of −8× Airy disk diameter to +8× Airy disk diameter with a step size of 2× Airy disk diameter in either the horizontal or vertical direction were used (tested in Subjects 1, 2 and 3). In 2 subjects, we also investigated the impact of diagonal offsets on visibility of obliquely oriented vessel walls (Subjects 1 and 2). 3. Finally, to evaluate robustness of a single horizontal offset of 8× Airy disk diameter, we tested imaging across larger regions of retina (tested in Subject 3). In pilot experiments, displacement of the small confocal aperture was investigated. We found that the detected intensity dropped very quickly, limiting the signal-to-noise ratio of the resulting images. Thus, we concentrated on measurements using displacements of the large aperture and do not report results for the displaced smaller aperture in this report.

2.4. Light levels and detector gain

All light levels were safe according to the American National Standards Institute ANSI Z136 [19]. The incident corneal power level of the infrared light source was set at 120 μW in five subjects and 70 μW in one subject (Fig. 1). Because the different conditions returned very different amounts of light to the detector, we needed to adjust the detector gain across conditions. In experiments directly comparing light return for all aperture conditions within a single session (performed in one subject, Fig. 1), we reduced the imaging beam power to 70 μW at the cornea to avoid saturating the detector for the aligned larger confocal aperture conditions. In general, for the variable offset experiment we found that the light return was too small for offsets greater than 8× the Airy disk diameter, i.e., displacements larger than the radius of the large aperture.

2.5. Imaging retinal locations

Comparisons were made for a variety of retinal locations in all 6 subjects, with each location imaged under the different aperture conditions. Comparisons of the impact of apertures on the images are based on comparisons within imaging sessions. To measure the possible interaction of aperture conditions with retinal structure we chose three template retinal regions, including regions where the RNFL was thick (e.g., the peripapillary region; the perifoveal region located 5°–10° from the fovea Fig. 1A), regions where the RNFL was thin

#173363 - $15.00 USD Received 2 Aug 2012; rev. 10 Sep 2012; accepted 10 Sep 2012; published 13 Sep 2012

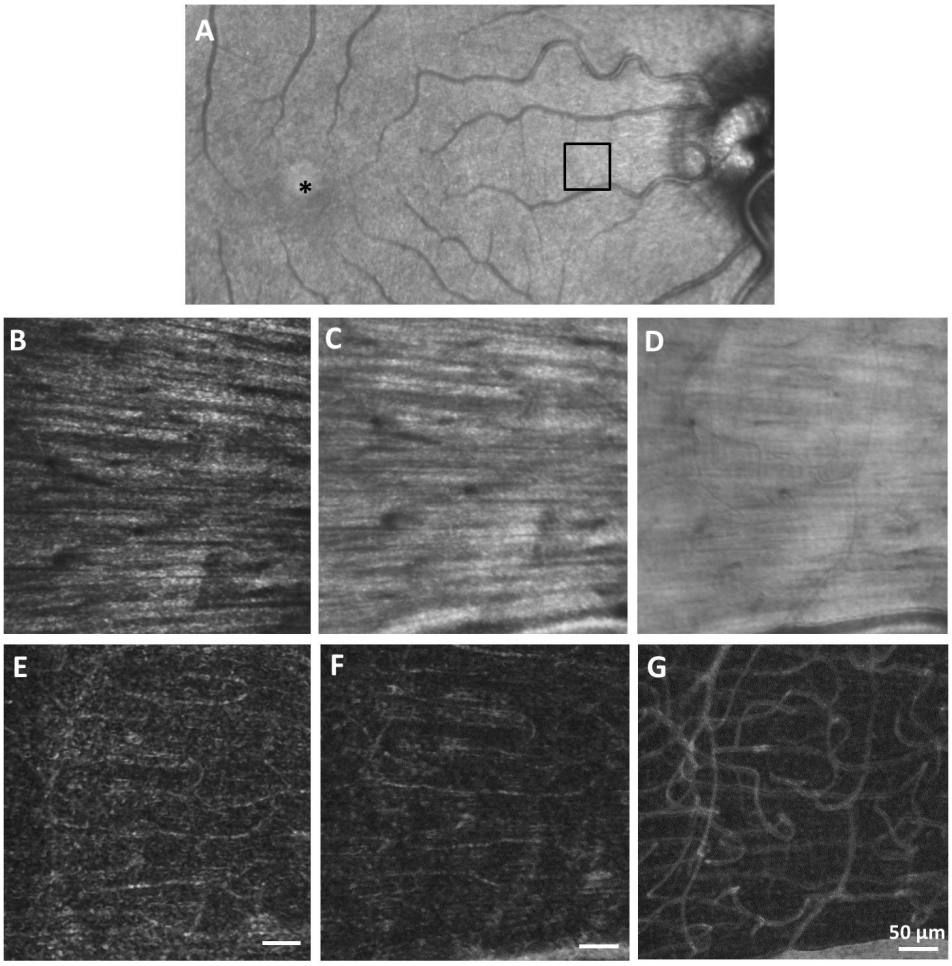

Fig. 1. The effect of aperture size and confocality on perifoveal microvasculature imaging. A, Spectralis infrared SLO fundus image of a 35 year old male. Asterisk indicates the fovea. The black box indicates the AOSLO imaging region located at ~10° from the fovea. B and C, AOSLO videos obtained using the small and large confocal apertures, respectively (Media 1 and Media 2), fine structures of the nerve fiber bundles were observed. However, capillaries were masked by the highly reflective nerve fiber layer. E and F, The corresponding standard error maps of B and C show a limited visibility of the capillaries. D, AOSLO video obtained using the large aperture with offset (6× Airy disk diameter horizontally and 4× Airy disk diameter vertically) (Media 3), capillaries were clearly seen due to the blockage of the direct specular reflection from the RNFL and increased detection of scattered light from the blood content. G, The standard error map calculated from the pre-truncated video of D.

and the outer retinal layer was thick (the foveal region), and finally regions where there is a great deal of scattering (the optic nerve head and the optic disc crescent).

2.6. Image acquisition and processing

AOSLO images of the retinal vascular network were collected as short sections of sequential video frames for all subjects. Typically a single acquisition of 100 frames (<4 seconds) at a single location and aperture condition was sufficient to collect a data set suitable for further image processing (Due to the maximum multimedia file size recommended by Biomedical Optics Express, all videos presented in this manuscript were truncated to less than 4 MB, approximately 25 frames/video). Imaging sessions were performed in one visit, which required approximately 30 minutes per subject. All images were corrected for the sinusoidal

#173363 - $15.00 USD Received 2 Aug 2012; rev. 10 Sep 2012; accepted 10 Sep 2012; published 13 Sep 2012

distortion created by the resonant galvanometer, and then aligned offline. Aligned image sequences were used to generate both average images and calculations of statistics on a pixel by pixel basis [5]. The primary calculated value were pixel standard error maps [5] where we use the temporal variation in image brightness arising from the motion of erythrocytes to detect the location of blood vessels. Montages were created using Adobe Photoshop CS5 (Adobe Systems Inc., San Jose, CA).

3. Results

3.1. The general effect of aperture size and aperture displacement

The contrast of different retinal structures varied markedly with the varying aperture conditions as shown in Fig. 1. For the small confocal aperture, the fine structures of the retinal nerve fiber bundles, and the superficial layer of capillaries were observed in high contrast when the appropriate retinal depth was optimally focused (Fig. 1B). For the large confocal apertures, these details were also visible although at somewhat lower contrast (Fig. 1C). However, with the large confocal aperture, the image has fewer specular highlights, presumably due to the larger contributions from scattered light. In general, for the centered confocal conditions, the deeper capillaries were not readily detected in the presence of strong contributions from the RNFL (Fig. 1B and 1C; Media 1 and Media 2). When the large aperture was offset, the specular component in the images decreased markedly, but blood vessels and erythrocytes were still readily detectable. However, in the absence of the more specular features, blood vessels and erythrocytes became a dominant feature of the image (Fig. 1D; Media 3). This general effect of displacement of the large aperture was observed in all subjects in all offset directions.

3.2. The relations of aperture displacement to retinal features

Varying the amount of offset of the large confocal aperture had a systematic impact on the appearance of retinal structures as shown in Fig. 2. Here we show sample data for four amounts of vertical displacements of the large confocal aperture (0, 2×, 6× and 8× the Airy disk diameter offset), together with pixel standard error maps for a retinal region containing a mid-sized retinal vein (~50 μm diameter). Figure 2 shows not only the vein, but several branch venules entering at an angle, and portions of the associated capillary network. As the large aperture was displaced, there were three major effects on the images. First, as mentioned, the specular highlights and non-vascular highlights in the images decreased, and the overall images consequently became more uniform (Fig. 2A, 2C, 2E, and 2G). Second, the vascular walls as shown in Fig. 2, became more visible orthogonal to the direction of displacement. The Michelson contrast of the vessel changed as indicated by the black arrow in Fig. 2A, with larger displacements having a higher contrast 62%, 61%, 76%, and 77% for the 0, 2×, 6× and 8× the Airy disk diameter offset, respectively. This general pattern of change was seen in all 3 subjects where the displacement was varied systematically. Third, the erythrocytes within the capillaries, while low in contrast became quite visible against the uniform background of the retina (Fig. 2G; Media 4). This impact on relative visibility of the erythrocytes is captured in the standard error maps (Fig. 2F, and 2H), which show the standard error of each pixel over time. For the centered aperture, the standard error map includes a large contribution from time variations in the more specular reflection (Fig. 2B), but with increasing displacement the capillary structure increasingly dominates the standard error maps, until for relatively large displacements (6× Airy disk diameter for instance), the variation from blood flow dominates the temporal brightness variations (Fig. 2G; Media 4). This relation between offset and retinal imaging was consistent in 3 subjects tested with systematic offsets.

#173363 - $15.00 USD Received 2 Aug 2012; rev. 10 Sep 2012; accepted 10 Sep 2012; published 13 Sep 2012

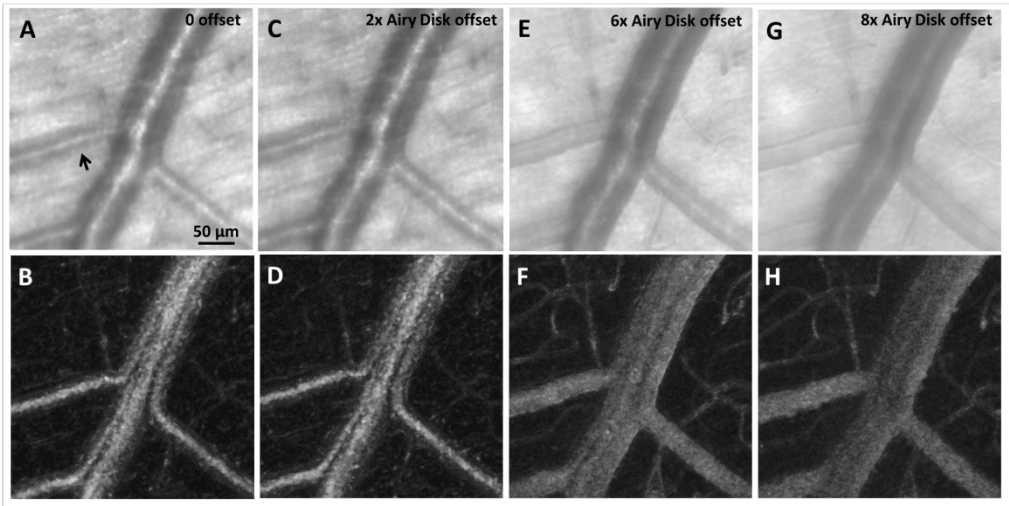

Fig. 2. The effect of varying confocality on retinal microvasculature imaging using the large aperture. Columns represent increasing amounts of vertical displacements of the aperture relative to the illumination spot. A, C, E, and G, Specular reflection from the RNFL decreases with increasing aperture displacement. Overall the reflectance image becomes more uniform in contrast and the erythrocytes within the capillaries become more visible with large displacement (Media 4). Michelson contrast was computed across the vessel wall as indicated by the black arrow in A (see text). B, D, F, and H, The standard error maps calculated from the pre-truncated videos for the conditions in the first row. Note the readily visible laminar flow pattern of erythrocytes in Media 4.

3.3. Variations in vascular imaging using offset apertures with retinal location

The use of a large confocal aperture provided a higher relative contrast for the motion of erythrocytes at all locations tested. It was possible to visualize the individual erythrocytes using a large offset aperture. Figure 3 (Media 5) shows an AOSLO registered video obtained at 1° from the optic nerve head using the large offset aperture. In general, the impact of offsetting the apertures was largest where the vasculature was collocated with highly scattering structures such as the RNFL. One example of this is the visualization of the peripapillary capillaries which nourish the retinal nerve fiber bundles. Using the offset apertures it was possible to image the entire peripapillary capillary network as shown in Fig. 4 for a region above the optic disc subtending approximately 5° × 5° in a 34 year old male. Here

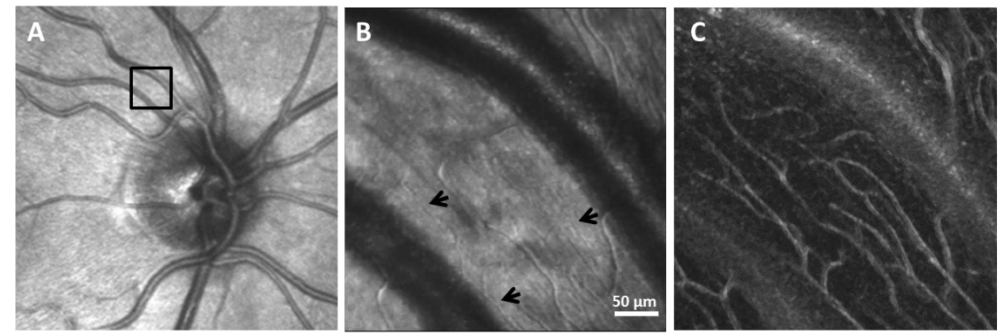

Fig. 3. A, Spectralis infrared SLO fundus image of a 24 year old male. The black box indicates the AOSLO imaging region located at 1° from the optic disc. B, AOSLO registered video obtained using a large offset aperture with 6× Airy disk diameter horizontally. Individual erythrocytes moving through the capillaries were clearly visualized as indicated by the black arrows (Media 5). C, The standard error map calculated from the pre-truncated Media 5 shows the peripapillary capillary network.

#173363 - $15.00 USD Received 2 Aug 2012; rev. 10 Sep 2012; accepted 10 Sep 2012; published 13 Sep 2012

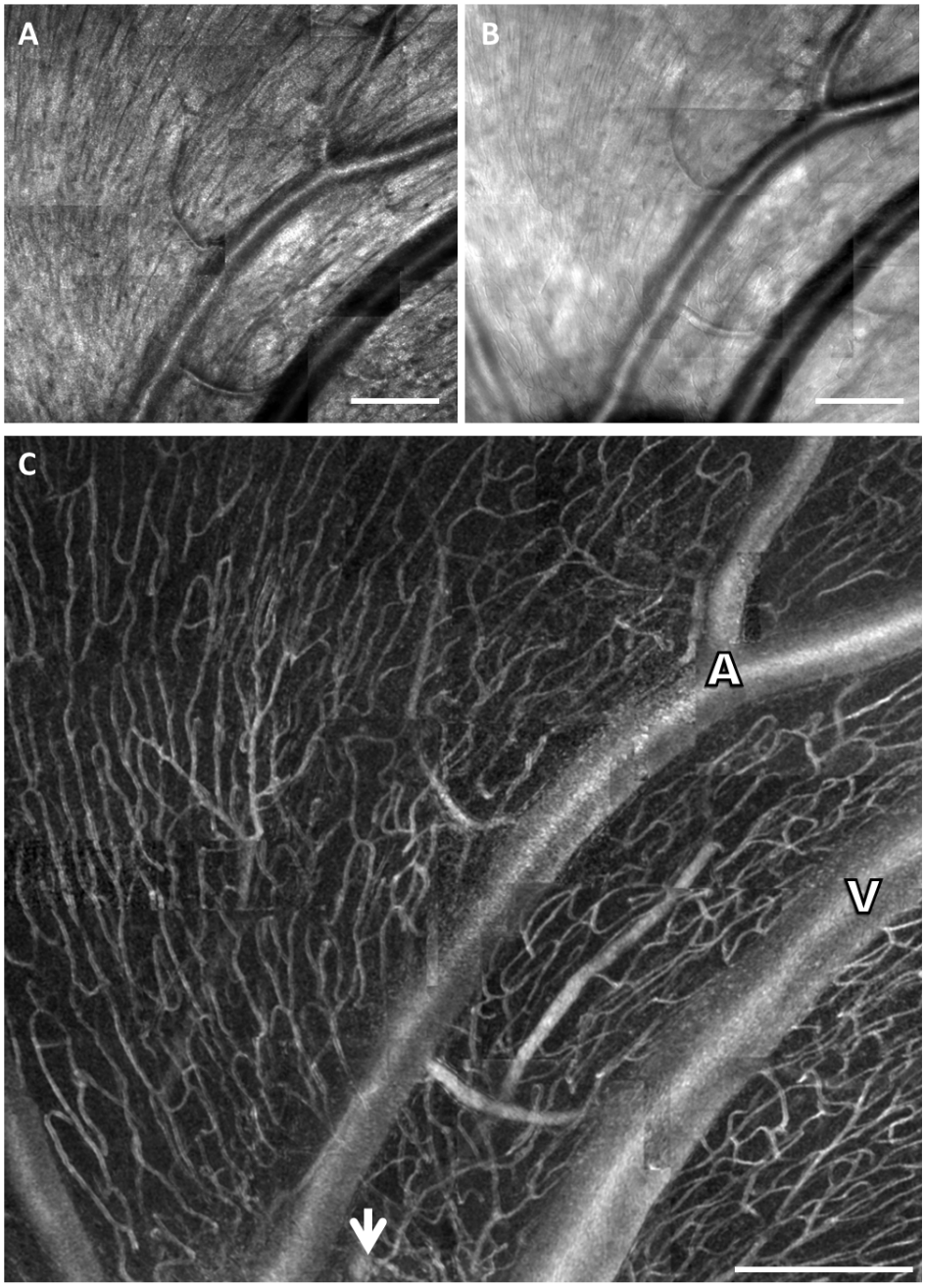

Fig. 4. 5° × 5° montages obtained from a location superior to the optic nerve head in a 34 year old male showing, A, peripapillary RNFL obtained using small confocal aperture and, B, peripapillary capillary network obtained using a large offset aperture at the same region. C, The standard error map calculated from the data shown as an average in B shows the peripapillary capillary network. Arrow indicates the optic disc margin. Artery and vein are labeled as "A" and "V', respectively. Scale bars = 300 µm.

we compare images obtained with the small confocal (Fig. 4A) and large offset aperture (Fig. 4B) as well as the standard error map (Fig. 4C) of the corresponding reflectance montage in Fig. 4B. Artery, vein, and the disc margin were identified by comparing the AOSLO images

#173363 - $15.00 USD Received 2 Aug 2012; rev. 10 Sep 2012; accepted 10 Sep 2012; published 13 Sep 2012

with the spectralis infrared SLO fundus picture. Note that capillaries running along the retinal nerve fiber bundles with complete connections between arterioles and venules clearly visualized in both the reflectance montage and the corresponding contrast enhanced standard error map. The capillary diameter varied from ~5 μm to 8 μm on the reflectance montage (Fig. 4B). For these conditions the AOSLO was focused at the RNFL and thus the montage shows only the superficial layer of retinal capillaries. This offset aperture technique was also tested at the foveal region, however, no noticeable improvement in capillary imaging was measured, except the appearance of the shadowing orthogonal to the offset direction was observed in this region with a thin RNFL.

3.4. The role of deeper retinal structure on visualization of the vasculature using offset apertures

The visibility of the erythrocytes and capillary vasculature was increased in regions with a strong scattering return from below the plane of focus, such as over the lamina cribrosa at the optic disc and at the optic disc crescent. The ability of the offset apertures to enhance visibility of the erythrocytes in the presence of light returning from the lamina cribrosa is shown in Fig. 5 (Media 6), where the microvasculature at the center of the optic disc was clearly visible using an 8× Airy disk diameter horizontal offset. The effect was especially striking when imaging at a region with peripapillary atrophy (e.g., the optic disc crescent), where there is a strong scattering source (the peripapillary atrophy) below the vascular layer. Figure 6 (Media 7) shows the complete capillary network above an optic disc crescent using

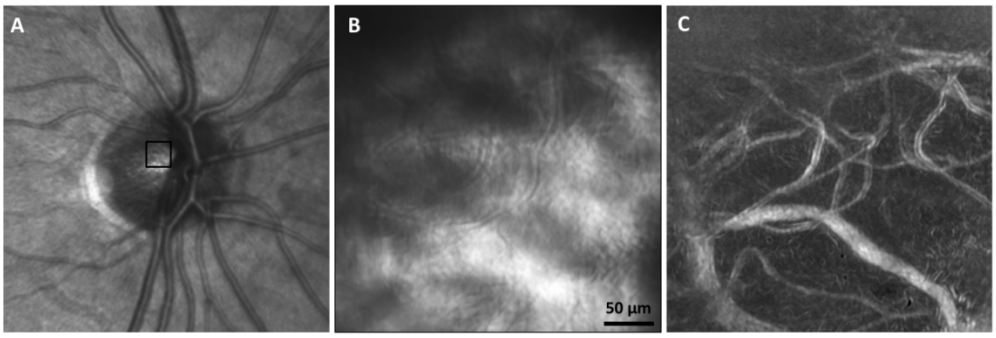

Fig. 5. A, Spectralis infrared SLO fundus image of a 22 year old male. The black box indicates the AOLSO imaging region located at the center of the disc. B, AOSLO registered video obtained at indicated region (Media 6). C, The standard error map calculated from the pre-truncated Media 6 showing the higher detectability of the flow over the lamina cribrosa.

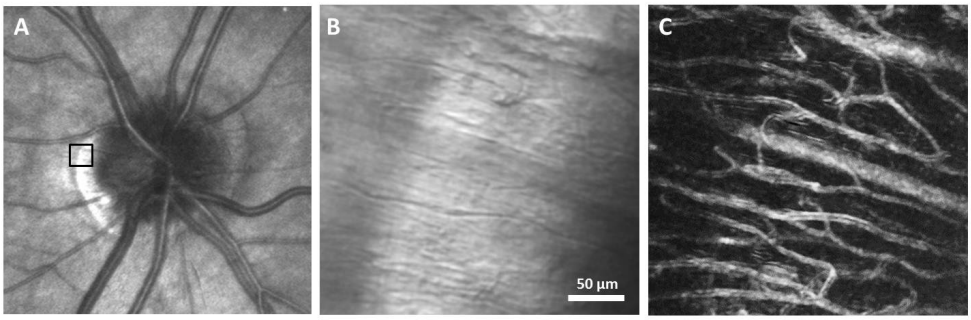

Fig. 6. A, Spectralis infrared SLO fundus image of a 25 year old male. The black box indicates the AOSLO imaging region located at the optic disc crescent B, AOSLO video obtained at indicated region (Media 7), blood vessels with various diameters were clearly visible. C, The standard error map calculated from the pre-truncated Media 7 showing the higher detectability of the flow over regions with highly scattering tissue below them.

#173363 - $15.00 USD Received 2 Aug 2012; rev. 10 Sep 2012; accepted 10 Sep 2012; published 13 Sep 2012

an offset aperture technique (horizontal offset = 6× Airy disk diameter). Here the contrast is higher over regions with a highly scattering region below them (the bright vertical stripe in the reflectance image, Fig. 6B). This effect was seen in all subjects that had a visible crescent of peripapillary atrophy using conventional imaging and has implications for understanding the mechanism for enhancing vascular visibility using offset apertures (see Discussion).

3.5. The effect of aperture offset on imaging the vascular fine structure

The use of an aperture offset also enhanced the visibility of the vessel walls (Fig. 7). This effect was especially prominent in examining the walls of the retinal arterioles. Improved visibility of the vessel walls was achieved by offsetting the aperture orthogonal to the side of the vessel wall. This effect was seen in all subjects. Figure 7A shows the inner and outer vessel wall linings in a peripapillary artery with a lumen diameter of ~110 µm located at 5° from the optic nerve head in a 35 year old male. The thickness of the vessel wall varies from 12 µm to 18 µm along the artery and the cellular structure of the vascular wall is readily visible. In general, three layers of the vessel wall were observed distinctively. Figure 7B shows an arteriole with 40 µm lumen diameter located at the optic disc crescent in a 26 year old female, again allowing the wall of the arteriole to be resolved.

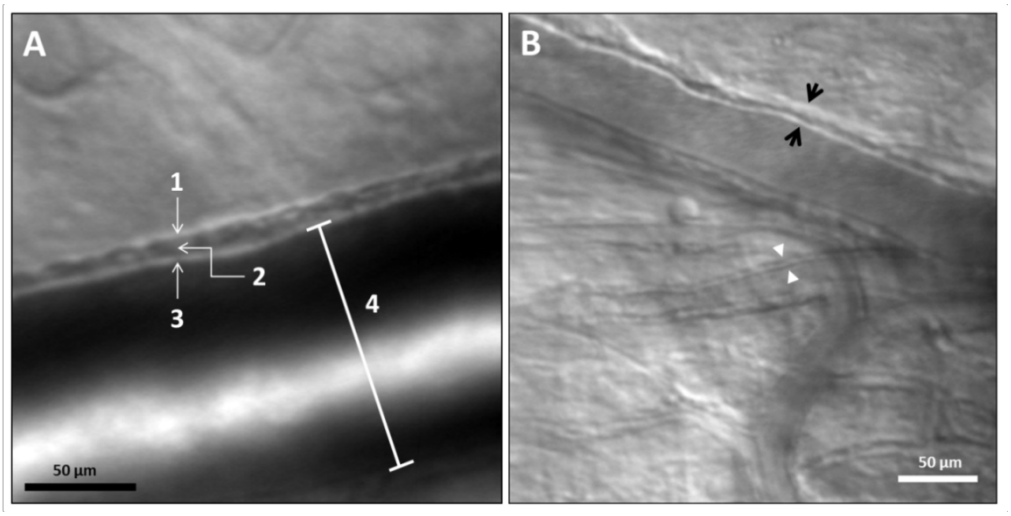

Fig. 7. Fine structure of peripapillary arterioles. A, A peripapillary arteriole located at 5° from the disc with a lumen diameter of 110 µm (Media 8) obtained with a displaced larger confocal aperture. White arrows indicate the three layers of the vessel wall. 1: Tunica adventitia; 2: Tunica media (smooth muscle); 3: Tunica intima. The thickness of the vessel wall varies from 12 to 18 µm along the vessel. 4: the lumen diameter of the peripapillary artery containing moving cells (Media 8). B, An arteriole with a 40 µm lumen diameter located at the optic disc crescent in a different subject (Media 9). The thickness of the vessel wall is 10 µm (black arrows) and 4.5 µm (white arrowheads) in the arteriole and its daughter branch, respectively.

4. Discussion

Our results indicate that some features of the retinal vascular network can be imaged better using a large displaced aperture than with a centered, small confocal aperture. The use of an offset aperture allows direct assessment of the structural and functional properties of the microvasculature in living human retina. Specifically, this approach allows us to routinely examine the substructure of the arteriole wall (Fig. 7) and to observe single file flow of erythrocytes (Media 4–8) in blood vessels, ranging in size from the largest peripapillary vessels to the smallest capillaries. This approach is quite different from most approaches which use singly backscattered light to visualize the vasculature.

#173363 - $15.00 USD Received 2 Aug 2012; rev. 10 Sep 2012; accepted 10 Sep 2012; published 13 Sep 2012

4.1. Comparisons of confocal and offset aperture imaging mode

The results of this study indicate that the imaging performance of an adaptive optics scanning laser ophthalmoscope can be tuned for imaging different types of retinal structures. While others have shown this is possible for cone imaging by selecting the light distribution in the pupil of the eye [20], the current study has concentrated on the use of controlling both the size and position of retinal conjugate apertures to select singly scattered and multiply scattered light. Detection of multiply scattered light has been shown to be valuable with the use of both aperture [15], polarization [21,22] and illuminant position [16] for traditional retinal imaging systems. Using an AOSLO we have also shown [23] that increasing aperture size can improve localization of subretinal changes. In the present study, we investigated the role of multiply scattered light by systematically changing the confocal aperture size and position, with an emphasis on structural imaging of the retinal microvasculture. This use of imaging using multiply scattered light improves the visibility of the microvasculature and erythrocytes through two mechanisms. The first, as shown in Fig. 1, is to decrease the relative contribution of structures that produce highly specular light returns such as the RNFL. The second appears to be capitalizing on the forward scattering of erythrocytes to enhance visualization relative to other retinal structures [24]. The importance of forward scattering is supported by our finding that highly scattering regions below the blood vessels increases contrast of erythrocytes for the offset aperture conditions (Fig. 3). Thus we posit a model that is shown schematically in Fig. 8. In the typical confocal imaging mode (Fig. 8A), while direct specular reflection from the RNFL (heavy arrows) and vasculature, returns back to the detector via the confocal aperture, the highly backscattering nature of the RNFL or other structures, dominates the resulting image. However, when the confocal aperture is displaced (Fig. 8B), we mask singly scattering light over most of the depth of focus of the system. The forward scattering from the focal volume however can be detected if it scatters a second (or third or more) times, such that it is returned within the focal volume of the system. While structures outside of the focal volume could also generate multiply scattered light that ultimately reaches the detector, it is only items that are near the focal point of the illuminating beam that will generate high spatial frequencies in the image. Thus, when focused at the level of the vasculature, the offset apertures provide excellent images of the retinal vasculature and erythrocytes.

The improvement of vascular contrast with multiply scattered light suggests that some of the same advantage could be obtained using a flood-illuminated AO system. Since such systems [25,26] can be simpler, since they do not require scanning and descanning, this approach might be simpler. It is not clear though that a flood system will provide the full benefits we describe for two reasons. First, since there is no aperture in a flood illuminated system, the possibility of decreasing a strong specular backscatter component is not present, although perhaps manipulation of pupil plane apertures could provide some of the benefit. Second, the small scanning beam provides a temporal separation of the scatter field, that is, for each location of the scanned beam, we are assigning the wide field of forward scattered light to that location, whereas in a flood illuminated system, all locations in the retina can contribute forward scattered light to a large area of the final image. In support of this advantage is the fact that to obtain our results required us to focus on the blood vessels themselves. Nevertheless, it is not clear that some of the advantages of the large aperture are not available to a flood illuminated system.

#173363 - $15.00 USD Received 2 Aug 2012; rev. 10 Sep 2012; accepted 10 Sep 2012; published 13 Sep 2012

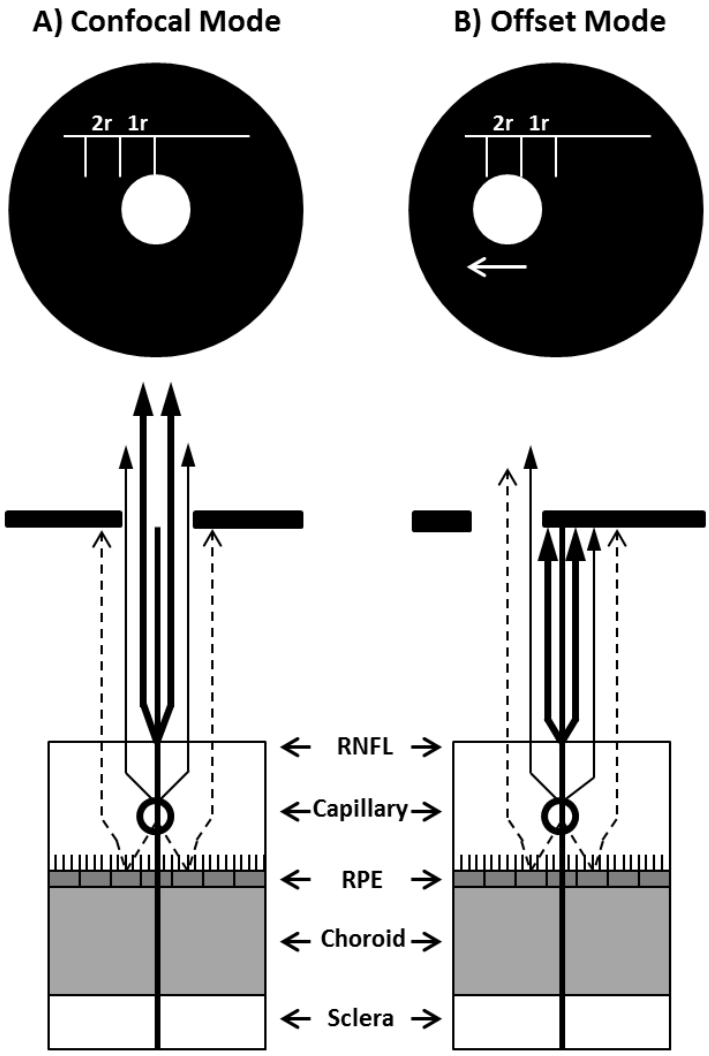

Fig. 8. Schematic diagram depicting the effect of offsetting the confocal aperture on the visibility of the capillaries. (A) A centered large aperture (10× the Airy disk diameter). Specular reflection from the RNFL (heavy arrows) decreases the contrast of the capillary. (B) Offset imaging mode with the confocal aperture displaced laterally with 1.5× radius. Specular reflection from the RNFL is blocked by the offset aperture, allowing more multiple scattered light (dashed arrows) to return back to the detector.

4.2. Imaging the peripapillary and papillary microvasculature

The offset aperture technique for vascular imaging is applicable to any retinal region within 20 degree of the fovea, including the peripapillary and papillary regions. Because it can be used to generate vascular maps with very high resolution, we can obtain images all the way to the optics disc or even within the disc. For instance, Fig. 4C shows the superficial layer of peripapillary capillaries running radially from the optic disc and parallel to the retinal nerve fiber bundles. This distinctive appearance is in agreement with previous histological studies in human eyes [27]. The entire superficial layer of the peripapillary capillary plexus is embedded within the RNFL. The ability of the offset apertures to enhance visibility of the erythrocytes in the presence of high reflection from other retinal structures was especially striking when imaging within the optic nerve head and optic disc crescent (Figs. 5 and 6). In this region

#173363 - $15.00 USD Received 2 Aug 2012; rev. 10 Sep 2012; accepted 10 Sep 2012; published 13 Sep 2012

confocal images are dominated by the strong scattering from the lamina cribrosa and the sclera, and larger confocal aperture images are dominated by scattering within the tissue (resulting in the classic "white" appearance of the optic nerve head and the optic disc crescent for flood illuminated imaging). Using an offset aperture however allowed us to select against the bright return and observe blood flow within the microvasculature located at the optic nerve head and optic disc crescent, as well as to map out the entire vascular network of the peripapillary and papillary regions (Fig. 5). These findings also support the forward scattering property of the blood content, particularly the erythrocytes.

4.3. Imaging the vascular fine structure

We also showed that the offset aperture technique allowed superb imaging of the vascular wall (Fig. 7). Consistent with previous histological measurements of vessel wall thickness in human retina [28], we measured that the vessel wall thickness was ~12–18 μm in an arteriole with ~110 μm luminal diameter. However, we were not able to resolve the venous vessel wall due to its relatively thin layer of smooth muscle (tunica media).

4.4. Future studies

This use of large offset apertures in an AOSLO, with or without standard error mapping has improved our ability to measure the retinal vasculature. A number of extensions of this technology are possible particularly with regard to normal retinal vascular physiology. The simplest would be to use an annular aperture. This would simplify the experiments and possibly provide enhanced vascular imaging for all vessel orientations simultaneously. An additional enhancement is to use the ability to visualize single file flow of erythrocytes to make accurate measurements of vessel diameters and simultaneously of plasma velocities using erythrocyte velocity as a surrogate for plasma flow velocity [29]. Accurate measurements will allow establishment of age, sex, and race related norms of both static and dynamic vascular properties. Additionally similar measurements and imaging can be done on virtually any retinal vascular pathology with special reference to the common conditions of hypertension, diabetes [30], and macular degeneration. Similarly, it is also likely that progressive changes occur in the papillary [31] and peripapillary [32,33] capillary network during the development of glaucoma. We anticipate that the freedom to do imaging of the retinal vasculature on a capillary level in the absence of the risks and burdens of fluorescein and with higher resolutions will yield considerable new scientifically and therapeutically valuable data.

5. Conclusions

In the present study, we introduce a direct and noninvasive imaging technique for imaging the microvasculature of the peripapillary, papillary, and perifoveal retina using offset apertures in an AOSLO. With this technique, we are able to demonstrate that by systematically altering the offset of a large confocal aperture, the flow through retinal vessels of various sizes can be visualized as well as the cross sectional structure of the arteriolar wall. Future studies of retinal capillary density, capillary blood flow analysis, blood vessel wall thickness and lumen diameter measurement are now possible using this imaging approach. While the current study used many frames of video at each location, we have found that acceptable capillary maps can be obtained with about 0.5 seconds per location.

Acknowledgments

The authors acknowledge Drs. Ann E Elsner and Thomas Gast for their helpful discussion. This work was supported by NIH grants R01-EY14375, R01-EY04395, and P30EY019008 to S. A. B, K23-EY017886 to D. A. V.

#173363 - $15.00 USD Received 2 Aug 2012; rev. 10 Sep 2012; accepted 10 Sep 2012; published 13 Sep 2012